J|A|C|S ARTICLES

Published on Web 04/07/2010

Yb@C_{2n} (n = 40, 41, 42): New Fullerene Allotropes with Unexplored Electrochemical Properties

Xing Lu,[†] Zdenek Slanina,[†] Takeshi Akasaka,*[,†] Takahiro Tsuchiya,[†] Naomi Mizorogi,[†] and Shigeru Nagase*[,‡]

Centre for Tsukuba Advanced Research Alliance, University of Tsukuba, Tsukuba, Ibaraki 305-8577, Japan, and Department of Theoretical and Computational Molecular Science, Institute for Molecular Science, Okazaki 444-8585, Japan

Received February 8, 2010; E-mail: akasaka@tara.tsukuba.ac.jp

Abstract: A series of ^{13}C-enriched monoytterbium endohedral metallofullerenes (EMFs)—Yb@C_{2n} (n = 40, 41, 42)—was synthesized and isolated. Their cage structures were systematically determined for the first time using computational and experimental ^{13}C NMR studies. The results revealed that all isomers adopt cage structures conforming to the isolated pentagon rule. In detail, Yb@C_{80} possesses the C_{2v}(3) cage; Yb@C_{82}(I, II, III) bear C_s(6), C_2(5), and C_{2v}(9) cages, respectively; and Yb@C_{84}(II, III, IV) have C_2(13), C_1(12), and C_2(11) cage structures, respectively. This is the first report describing C_2(13)-C_{84} and C_1(12)-C_{84} cage structures. It is noteworthy that the cage structures found for mono-EMFs generally differ from either the corresponding empty fullerenes or the related EMFs encapsulating more than one metal atom, indicating that the metal atom inside the fullerene cage plays an important role in determining the EMF structure. On the basis of the fact that the structure of Yb@C_2(13)-C_{84} resembles that of Yb@C_2(5)-C_{82}, a metal-templated growth process was proposed as a kinetic factor controlling EMF formation. Furthermore, previous electrochemical studies of divalent EMFs have failed to observe their oxidation potentials, which have raised the assumption that such species are large-bandgap molecules. This study revealed that all isomers of Yb@C_{2n} (n = 40, 41, 42) display one or two reversible oxidation steps together with four reversible reduction processes in 1,2-dichlorobenzene, even at a low scan rate (20 mV/s), which enables estimation of their electrochemical bandgaps ($\Delta E = {}^{ox}E_1 - {}^{red}E_1$). The results show a ΔE value of 0.88−1.41 V for Yb@C_{2n} ($2n$ = 40, 41, 42), which is much larger than the values of trivalent mono-EMFs (ΔE < 0.5 V), but generally smaller than those of metal nitride cluster EMFs (1.4 V < ΔE < 2.1 V). Results further demonstrated that the ΔE values correlate reasonably with their relative abundances.

1. Introduction

The capability of fullerenes to encapsulate metal atom(s) inside their hollow cavities was realized[1] only days after the first recognition of the "soccer ball" structure of C_{60} in 1985[2] and was further proved by the successful extraction of La@C_{82} in 1991.[3] Thereafter, great efforts have been made to incarcerate various metallic elements inside the cavity of fullerenes. It gradually turned out that only the metal elements of groups 2, 3, 4, and 5 in the periodic table can be imprisoned within fullerenes during the most effective arc-discharging process.[4−7] The presence of a metallic species and its strong interactions with the fullerene cage produce unique structures, fascinating properties, and vast potential applications in electronics, photovoltaics, biomedicine, and materials science of this new class of molecules, which are now commonly called endohedral metallofullerenes (EMFs).[4−7]

Regarding the number of metals encapsulated inside the fullerene cage, it can be concluded from published results that one metal atom is always simply jailed by a fullerene cage, whereas three to four metal atoms, when encapsulated, normally demand nonmetallic elements as a stabilizer by forming metallic clusters.[4−7] Representative examples of cluster EMFs with three or four metals are Sc_3N@C_{80},[8] Sc_3C_2@C_{80},[9] and Sc_4O_2@C_{80}.[10]

[†] University of Tsukuba.
[‡] Institute for Molecular Science.

(1) Heath, J. R.; O'Brien, S. C.; Zhang, Q.; Liu, Y.; Curl, R. F.; Kroto, H. W.; Tittel, F. K.; Smalley, R. E. *J. Am. Chem. Soc.* **1985**, *107*, 7779–7780.
(2) Kroto, H. W.; Heath, J. R.; Obrien, S. C.; Curl, R. F.; Smalley, R. E. *Nature* **1985**, *318*, 162–163.
(3) Chai, Y.; Guo, T.; Jin, C. M.; Haufler, R. E.; Chibante, L. P. F.; Fure, J.; Wang, L. H.; Alford, J. M.; Smalley, R. E. *J. Phys. Chem.* **1991**, *95*, 7564–7568.
(4) *Endofullerenes: A New Family of Carbon Clusters*; Akasaka, T., Nagase, S., Eds.; Kluwer: Dordrecht, The Netherlands, 2002.
(5) Lu, X.; Akasaka, T.; Nagase, S. Rare Earth Metals Trapped inside Fullerenes−Endohedral Moallofullerenes. In *Rare Earth Coordination Chemistry: from Basic to Applications*; Huang, C. H., Ed.; John Wiley & Sons: Singapore, 2010.
(6) Dunsch, L.; Yang, S. *Small* **2007**, *3*, 1298–1320.
(7) Chaur, M. N.; Melin, F.; Ortiz, A. L.; Echegoyen, L. *Angew. Chem., Int. Ed.* **2009**, *48*, 7514–7538.
(8) Stevenson, S.; Rice, G.; Glass, T.; Harich, K.; Cromer, F.; Jordan, M. R.; Craft, J.; Hadju, E.; Bible, R.; Olmstead, M. M.; Maitra, K.; Fisher, A. J.; Balch, A. L.; Dorn, H. C. *Nature* **1999**, *401*, 55–57.
(9) Iiduka, Y.; Wakahara, T.; Nakahodo, T.; Tsuchiya, T.; Sakuraba, A.; Maeda, Y.; Akasaka, T.; Yoza, K.; Horn, E.; Kato, T.; Liu, M. T. H.; Mizorogi, N.; Kobayashi, K.; Nagase, S. *J. Am. Chem. Soc.* **2005**, *127*, 12500–12501.
(10) Stevenson, S.; Mackey, M. A.; Stuart, M. A.; Phillips, J. P.; Easterling, M. L.; Chancellor, C. J.; Olmstead, M. M.; Balch, A. L. *J. Am. Chem. Soc.* **2008**, *130*, 11844–11845.

10.1021/ja101131e

As a transition, two metal atoms can be encapsulated either as a dimer or in the form of metal carbide such as $Y_2@C_{82}$ and $Y_2C_2@C_{82}$.[11] Although cluster EMFs, especially the so-called trimetallic nitride template (TNT) family with its outstanding representative $Sc_3N@C_{80}$, have recently attracted considerable attention because of their high production yield and high stability resulting from strong metal−cage interactions,[6−8] mono-EMFs, i.e., fullerenes with only one metal atom inside, however, are viewed as the simplest prototypes of EMFs with high academic and practical values for revealing the structures, properties, and formation mechanisms of EMFs.[4,5] Consequently, mono-EMFs serve as a bridge linking empty fullerenes with EMFs encapsulating two metal atoms or a metallic cluster.[4−7]

Electron transfer from the encapsulated metallic species to the fullerene cage takes place in EMFs.[4,5] For mono-EMFs, three electrons are transferred from the encaged metal to the fullerene cage when Sc, Y, and most lanthanides (La, Ce, Pr, Nd, Gd, Tb, Dy, Ho, Er, and Lu) are encapsulated.[5] However, Sm, Eu, Tm, Yb, and alkaline earth metals (Ca, Sr, Ba) donate only two electrons and prefer to take a valence of +2. Consequently, the EMFs containing one metal are classified into two categories, trivalent EMFs and divalent EMFs, according to the electronic state of the encaged metal.[12] These two categories of EMFs differ remarkably from each other in terms of molecular structures and intrinsic properties. In particular, the yield of divalent EMFs is much lower than that of the trivalent ones,[12] resulting in the fact that divalent EMFs have been little studied. However, the isomerism of divalent EMFs is normally more diverse,[13−16] thereby providing additional opportunities for investigating the structures, metal−cage interactions, physical and chemical properties, and potential applications of EMFs.

Because of the particularly low production yield, ytterbium-containing EMFs were not successfully isolated until 2004, when Xu et al. added nickel as a catalyst to promote the yield.[17] Consequently, several species of Yb-EMFs were isolated and characterized with vis−NIR spectrometry and electrochemical methods.[17,18] However, because of the scarcity of samples, cage structures of Yb-EMFs are rarely reported.[19]

In this article, ^{13}C-enriched carbon and $YbNi_2$ alloy were used to synthesize Yb-EMFs,[20] and a series of Yb-EMFs, namely, $Yb@C_{80}$, $Yb@C_{82}$(I, II, III), and $Yb@C_{84}$(I, II, III, IV), were isolated. By virtue of the high ^{13}C ratio of up to 15%, we obtained high-resolution ^{13}C NMR spectra and assigned their cage structures (except for $Yb@C_{84}$(I) because of its extremely low yield). Moreover, we succeeded, for the first time, in obtaining the oxidation potentials of divalent EMFs, discovering that their electrochemical bandgaps are reasonably correlated to the relative abundances.

Ytterbium was chosen in this work for two reasons. First, Yb-EMFs are the latest isolated among EMFs containing lanthanide metals; accordingly, they have received little attention. For that reason, it is meaningful to undertake an in-depth investigation of the structures and properties of Yb-EMFs.[17−19] Second and more importantly, Yb-EMFs are rather suitable for ^{13}C NMR measurements. As described above, Yb transfers two electrons to the fullerene cage. Consequently, the resulting molecules are diamagnetic and can therefore be subjected directly to NMR measurement. However, trivalent mono-EMFs, such as $M@C_{82}$ (M = Y, La, Ce, Pr, etc.), are unsuitable for direct NMR measurement because of their paramagnetic nature.[21−26] As a result, NMR spectroscopy was performed only on their anions.[22−26] Furthermore, after transferring two electrons, Yb^{2+} is diamagnetic, so that the ^{13}C NMR signals of these Yb-EMFs all appear in the aromatic region. However, anisotropic magnetic behaviors of cage carbons induced by the paramagnetic Tm^{2+} have been observed for the three isomers of $Tm@C_{82}$, which made their ^{13}C NMR patterns complicated and the assignments of the ^{13}C NMR signals difficult.[27] Similar phenomena were also observed for Ce- and Pr-containing EMFs.[28−30]

2. Experimental Section

Soot containing ^{13}C-enriched Yb-EMFs was synthesized using the direct current (dc) arc discharge method.[19,20] Briefly, a core-drilled graphite rod filled with ^{13}C amorphous carbon/$YbNi_2$ (atomic ratio = 10:1) was burned under 150 Torr floating helium atmosphere with a power of 100 A × 40 V. The soot was collected and refluxed in 1,2,4-trichlorobenzene (TCB) under a nitrogen atmosphere for 15 h. After removal of TCB, the residue was dissolved in toluene and subjected to HPLC separation using procedures similar to those reported by Xu et al.[19] However, because of the presence of reactive dichlorophenyl radical in TCB during reflux,[31−33] we did not find abundant pristine $Yb@C_{2n}$ (n = 37, 38, 39) but indeed observed their dichlorophenyl derivatives, which will be reported separately once complete separations and full characterizations are fulfilled. The purity of the isolated isomers of $Yb@C_{2n}$ (n = 40, 41, 42)

(11) Inoue, T.; Tomiyama, T.; Sugai, T.; Okazaki, T.; Suematsu, T.; Fujii, N.; Utsumi, H.; Nojima, K.; Shinohara, H. *J. Phys. Chem. B* **2004**, *108*, 7573–7579.
(12) Huang, H. J.; Yang, S. H. *J. Phys. Chem. B* **1998**, *102*, 10196–10200.
(13) Xu, Z. D.; Nakane, T.; Shinohara, H. *J. Am. Chem. Soc.* **1996**, *118*, 11309–11310.
(14) Dennis, T. J. S.; Shinohara, H. *Chem. Commun.* **1998**, 883–884.
(15) Okazaki, T.; Lian, Y. F.; Gu, Z. N.; Suenaga, K.; Shinohara, H. *Chem. Phys. Lett.* **2000**, *320*, 435–440.
(16) Kirbach, U.; Dunsch, L. *Angew. Chem., Int. Ed.* **1996**, *35*, 2380–2383.
(17) Xu, J. X.; Lu, X.; Zhou, X. H.; He, X. R.; Shi, Z. J.; Gu, Z. N. *Chem. Mater.* **2004**, *16*, 2959–2964.
(18) Xu, J. X.; Li, M. X.; Shi, Z. J.; Gu, Z. N. *Chem.−Eur. J.* **2006**, *12*, 562–567.
(19) (a) Xu, J. X.; Tsuchiya, T.; Hao, C.; Shi, Z. J.; Wakahara, T.; Mi, W. H.; Gu, Z. N.; Akasaka, T. *Chem. Phys. Lett.* **2006**, *419*, 44–47. (b) Slanina, Z.; Uhlik, F.; Nagase, S. *J. Phys. Chem. A* **2006**, *110*, 12860–12863.
(20) Yamazaki, Y.; Nakajima, K.; Wakahara, T.; Tsuchiya, T.; Ishitsuka, M. O.; Maeda, Y.; Akasaka, T.; Waelchli, M.; Mizorogi, N.; Nagase, S. *Angew. Chem., Int. Ed.* **2008**, *47*, 7905–7908.
(21) Kobayashi, K.; Nagase, S. *Chem. Phys. Lett.* **1998**, *282*, 325–329.
(22) Akasaka, T.; Okubo, S.; Kondo, M.; Maeda, Y.; Wakahara, T.; Kato, T.; Suzuki, T.; Yamamoto, K.; Kobayashi, K.; Nagase, S. *Chem. Phys. Lett.* **2000**, *319*, 153–156.
(23) Akasaka, T.; et al. *J. Am. Chem. Soc.* **2000**, *122*, 9316–9317.
(24) Akasaka, T.; Wakahara, T.; Nagase, S.; Kobayashi, K.; Waelchli, M.; Yamamoto, K.; Kondo, M.; Shirakura, S.; Maeda, Y.; Kato, T.; Kako, M.; Nakadaira, Y.; Gao, X.; Van Caemelbecke, E.; Kadish, K. M. *J. Phys. Chem. B* **2001**, *105*, 2971–2974.
(25) Wakahara, T.; Okubo, S.; Kondo, M.; Maeda, Y.; Akasaka, T.; Waelchli, M.; Kako, M.; Kobayashi, K.; Nagase, S.; Kato, T.; Yamamoto, K.; Gao, X.; Van Caemelbecke, E.; Kadish, K. M. *Chem. Phys. Lett.* **2002**, *360*, 235–239.
(26) Wakahara, T.; Kobayashi, J.; Yamada, M.; Maeda, Y.; Tsuchiya, T.; Okamura, M.; Akasaka, T.; Waelchli, M.; Kobayashi, K.; Nagase, S.; Kato, T.; Kako, M.; Yamamoto, K.; Kadish, K. M. *J. Am. Chem. Soc.* **2004**, *126*, 4883–4887.
(27) Kodama, T.; Ozawa, N.; Miyake, Y.; Sakaguchi, K.; Nishikawa, H.; Ikemoto, I.; Kikuchi, K.; Achiba, Y. *J. Am. Chem. Soc.* **2002**, *124*, 1452–1455.
(28) Yamada, M.; Wakahara, T.; Lian, Y. F.; Tsuchiya, T.; Akasaka, T.; Waelchli, M.; Mizorogi, N.; Nagase, S.; Kadish, K. M. *J. Am. Chem. Soc.* **2006**, *128*, 1400–1401.
(29) Takano, Y.; Aoyagi, M.; Yamada, M.; Nikawa, H.; Slanina, Z.; Mizorogi, N.; Ishitsuka, M. O.; Tsuchiya, T.; Maeda, Y.; Akasaka, T.; Kato, T.; Nagase, S. *J. Am. Chem. Soc.* **2009**, *131*, 9340–9346.
(30) Plant, S. R.; Ng, T. C.; Warner, J. H.; Dantelle, G.; Ardavan, A.; Briggs, G. A. D.; Porfyrakis, K. *Chem. Commun.* **2009**, 4082–4084.

under study was estimated to be higher than 99% according to the HPLC and mass spectrometric results (Figures S2 and S3), as well as the ^{13}C NMR and electrochemical results shown below.

^{13}C amorphous carbon (99%) was bought from Cambridge Isotope Laboratories Inc. Core-drilled graphite rods (Φ 35 × 150 mm) were produced by Toyo Tanso Co. Ltd. Preparative HPLC was conducted on an LC-908 machine (Japan Analytical Industry Co. Ltd.) with toluene as the mobile phase. Matrix-assisted laser decomposition/ionization time-of-flight (MALDI-TOF) mass spectrometry was performed using a BIFLEX III mass spectrometer (Bruker Analytik, Germany) with 1,1,4,4-tetraphenyl-1,3-butadiene as matrix. UV−vis−NIR spectra were measured on a UV 3150 spectrometer (Shimadzu Corp., Japan) in CS_2. The ^{13}C NMR spectra were recorded with an Avance-500 spectrometer (Bruker Analytik, Germany) in CS_2 with acetone-d_6 external lock; all chemical shifts were calibrated according to the peak of TMS ($\delta = 0$ ppm). Cyclic voltammograms (CV) and differential pulse voltammograms (DPV) were obtained in 1,2-dichlorobenzene (ODCB) with 0.1 M $(n\text{-Bu})_4NPF_6$ at a Pt working electrode on a potentiostat/galvanostat workstation (CV-50W, BAS Inc.). The scan rate of CV was 20 mV/s. Conditions of DPV were 50 mV pulse amplitude and 20 mV/s scan rate.

3. Results and Discussion

3.1. Cage Structures. 3.1.1. General Considerations. Fullerene cages containing fused pentagons, which violate the isolated pentagon rule (IPR), are frequently found among EMFs.[34−38] According to Fu et al., the highly pyramidalized [5,5]-carbons of fused pentagons invariably display highly deshielded ^{13}C NMR resonances at higher than 155 ppm.[39] Consequently, non-IPR structures can be excluded from the Yb@C_{2n} ($n = 40, 41, 42$) isomers in this study because no ^{13}C NMR signal higher than 155 ppm was observed. Accordingly, the vast majority of non-IPR isomers of C_{2n} ($n = 40, 41, 42$) are not considered; only the short-term numbering system in accordance with the Fowler−Manolopoulos spiral algorithm[40] is adopted to label these isomers.

Furthermore, it has been found that two carbon atoms can be encapsulated inside the fullerene cage together with two, three, or four metal atoms, forming metal carbide cluster EMFs.[9,11,20] Yamazaki et al. reported that the encapsulated C_2 moieties in ^{13}C-enriched $Sc_2C_2@C_{3v}(8)$-C_{82}, $Sc_2C_2@D_{2d}(23)$-C_{84}, and $[Sc_3C_2@I_h(7)\text{-}C_{80}]^-$ respectively give rise to ^{13}C NMR signals at 253.2, 249.2, and 328.3 ppm.[20] In this study, no signal between 200 and 400 ppm was observed. It is therefore safe to conclude that only one Yb atom is encapsulated in the fullerene cage. Actually, no example of cluster EMFs containing only one metal atom has been reported, which implies that one metal atom is insufficient to stabilize the whole cluster.[5]

All isomers of Yb@C_{2n} in this study exhibit ^{13}C NMR resonances in the aromatic region (155−125 ppm); only coincident overlaps of the resonances from the samples are observed. The expanded ^{13}C NMR spectra and detailed assignments of the resonances are presented in the Supporting Information (Figures S6−S13, Table S1).

Theoretical calculations were conducted to aid secure assignment of the cage structures. All calculations were conducted using the Gaussian 03 program package.[41] The molecular structures were first optimized at the B3LYP/3-21G-CEP level (3-21G basis set for C atoms and CEP-4G basis with the CEP effective core potential (ECP) for Yb) and then reoptimized with the B3LYP/6-31G*-SDD approach (6-31G* basis for C and SDD basis with the SDD ECP for Yb), both with the B3LYP density functional.[42] Energy minima were checked using B3LYP/3-21G-CEP vibrational analysis. Relative energies and ^{13}C NMR spectra were calculated at the B3LYP/6-311G*-SDD level with all chemical shift values calibrated to the observed C_{60} line of 143.15 ppm. Ionization potentials and electron affinities were evaluated using the B3LYP/6-31+G*∼SDD treatment.[42]

3.1.2. Cage Structure of Yb@C_{80}. Seven isomers of C_{80} satisfy the IPR, but only two with a $D_2(2)$[43] or a $D_{5d}(1)$[44] symmetry were isolable for pristine C_{80}. A recent example of empty C_{80} is the insoluble $C_{2v}(5)$ isomer isolated as trifluoromethyl derivatives.[45] Interestingly, when two metal atoms (such as La_2) or a metal cluster (such as Sc_3N) is encapsulated by a C_{80} cage, the two cage structures $I_h(7)$ and $D_{5h}(6)$ become the most stable, although they are not preferred by empty C_{80}.[46−48] This is explained by the 6-fold electron transfer from the incarcerated metallic species to the fullerene cage, which renders

(31) Nikawa, H.; Kikuchi, T.; Wakahara, T.; Nakahodo, T.; Tsuchiya, T.; Rahman, G. M. A.; Akasaka, T.; Maeda, Y.; Yoza, K.; Horn, E.; Yamamoto, K.; Mizorogi, N.; Nagase, S. *J. Am. Chem. Soc.* **2005**, *127*, 9684–9685.

(32) Wakahara, T.; Nikawa, H.; Kikuchi, T.; Nakahodo, T.; Rahman, G. M. A.; Tsuchiya, T.; Maeda, Y.; Akasaka, T.; Yoza, K.; Horn, E.; Yamamoto, K.; Mizorogi, N.; Slanina, Z.; Nagase, S. *J. Am. Chem. Soc.* **2006**, *128*, 14228–14229.

(33) Nikawa, H.; Yamada, T.; Cao, B. P.; Mizorogi, N.; Slanina, Z.; Tsuchiya, T.; Akasaka, T.; Yoza, K.; Nagase, S. *J. Am. Chem. Soc.* **2009**, *131*, 10950–10954.

(34) Wang, C. R.; Kai, T.; Tomiyama, T.; Yoshida, T.; Kobayashi, Y.; Nishibori, E.; Takata, M.; Sakata, M.; Shinohara, H. *Nature* **2000**, *408*, 426–427.

(35) Stevenson, S.; Fowler, P. W.; Heine, T.; Duchamp, J. C.; Rice, G.; Glass, T.; Harich, K.; Hajdu, E.; Bible, R.; Dorn, H. C. *Nature* **2000**, *408*, 427–428.

(36) Lu, X.; Nikawa, H.; Nakahodo, T.; Tsuchiya, T.; Ishitsuka, M. O.; Maeda, Y.; Akasaka, T.; Toki, M.; Sawa, H.; Slanina, Z.; Mizorogi, N.; Nagase, S. *J. Am. Chem. Soc.* **2008**, *130*, 9129–9136.

(37) Lu, X.; Nikawa, H.; Tsuchiya, T.; Maeda, Y.; Ishitsuka, M. O.; Akasaka, T.; Toki, M.; Sawa, H.; Slanina, Z.; Mizorogi, N.; Nagase, S. *Angew. Chem., Int. Ed.* **2008**, *47*, 8642–8645.

(38) Beavers, C. M.; Chaur, M. N.; Olmstead, M. M.; Echegoyen, L.; Balch, A. L. *J. Am. Chem. Soc.* **2009**, *131*, 11519–11524.

(39) Fu, W. J.; Xu, L. S.; Azurmendi, H.; Ge, J. C.; Fuhrer, T.; Zuo, T. M.; Reid, J.; Shu, C. Y.; Harich, K.; Dorn, H. C. *J. Am. Chem. Soc.* **2009**, *131*, 11762–11769.

(40) *An Atlas of Fullerenes*; Fowler, P. W., Manolopoulos, D. E., Eds.; Clarendon Press: Oxford, 1995.

(41) Frisch, M. J.; et al. *GAUSSIAN 03, Revision C. 01*; Gaussian Inc.: Wallingford, CT, 2004.

(42) (a) Becke, A. D. *Phys. Rev. A* **1988**, *38*, 3098–3100. (b) Becke, A. D. *J. Chem. Phys.* **1993**, *98*, 5648–5652. (c) Lee, C.; Yang, W.; Parr, R. G. *Phys. Rev. B* **1988**, *37*, 785–789. (d) Cundari, T. R.; Stevens, W. J. *J. Chem. Phys.* **1993**, *98*, 5555–5565. (e) Cao, X. Y; Dolg, M. *J. Mol. Struct. (THEOCHEM)* **2002**, *581*, 139–147. (f) Hay, P. J; Wadt, W. R. *J. Chem. Phys.* **1985**, *82*, 299–310. (g) Hehre, W. J; Ditchfield, R; Pople, J. A. *J. Chem. Phys.* **1972**, *56*, 2257–2261. (h) Wolinski, K; Hilton, J. F; Pulay, P. *J. Am. Chem. Soc.* **1990**, *112*, 8251–8260. (i) Sun, G. Y; Kertesz, M. *J. Phys. Chem. A* **2000**, *104*, 7398–7403.

(43) Hennrich, F. H.; Michel, R. H.; Fischer, A.; Richard Schneider, S.; Gilb, S.; Kappes, M. M.; Fuchs, D.; Burk, M.; Kobayashi, K.; Nagase, S. *Angew. Chem., Int. Ed. Engl.* **1996**, *35*, 1732–1734.

(44) Wang, C. R.; Sugai, T.; Kai, T.; Tomiyama, T.; Shinohara, H. *Chem. Commun.* **2000**, 557–558.

(45) Shustova, N. B.; Kuvychko, I. V.; Bolskar, R. D.; Seppelt, K.; Strauss, S. H.; Popov, A. A.; Boltalina, O. V. *J. Am. Chem. Soc.* **2006**, *128*, 15793–15798.

(46) Akasaka, T.; Nagase, S.; Kobayashi, K.; Walchli, M.; Yamamoto, K.; Funasaka, H.; Kako, M.; Hoshino, T.; Erata, T. *Angew. Chem., Int. Ed. Engl.* **1997**, *36*, 1643–1645.

(47) Duchamp, J. C.; Demortier, A.; Fletcher, K. R.; Dorn, D.; Iezzi, E. B.; Glass, T.; Dorn, H. C. *Chem. Phys. Lett.* **2003**, *375*, 655–659.

(48) Zuo, T. M.; Olmstead, M. M.; Beavers, C. M.; Balch, A. L.; Wang, G. B.; Yee, G. T.; Shu, C. Y.; Xu, L. S.; Elliott, B.; Echegoyen, L.; Duchamp, J. C.; Dorn, H. C. *Inorg. Chem.* **2008**, *47*, 5234–5244.

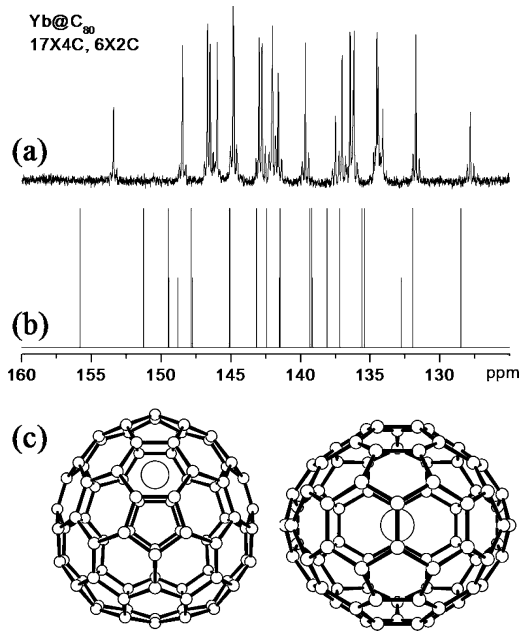

Figure 1. (a) ^{13}C NMR spectrum of Yb@C_{80} showing a 17 × 4C, 6 × 2C pattern. (b) Calculated ^{13}C NMR spectrum of Yb@$C_{2v}(3)$-C_{80}. (c) Optimized structure of Yb@$C_{2v}(3)$-C_{80} (left, side view; right, top view).

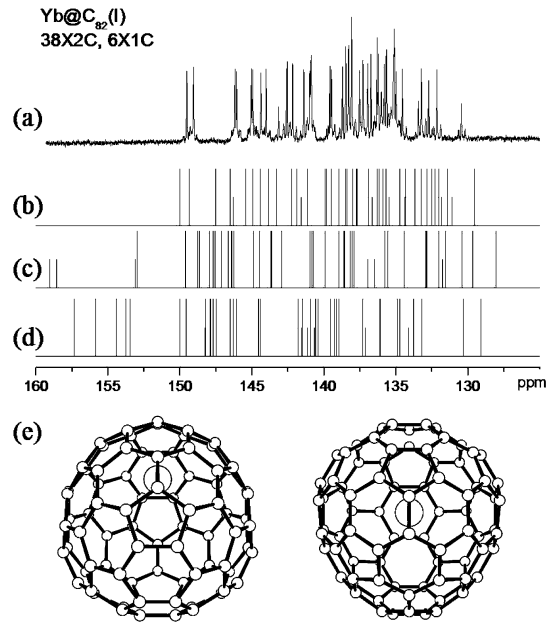

Figure 2. (a) ^{13}C NMR spectrum of Yb@C_{82}(I) with a 38 × 2C, 6 × 1C pattern. (b) Calculated ^{13}C NMR spectrum of Yb@$C_s(6)$-C_{82}, which is the most stable C_s isomer. (c) Calculated ^{13}C NMR spectrum of Yb@$C_s(4)$-C_{82}, which is 52.5 kJ/mol less stable than the $C_s(6)$ isomer. (d) Calculated ^{13}C NMR spectrum of Yb@$C_s(2)$-C_{82}, which is 96.3 kJ/mol less stable than the $C_s(6)$ isomer. (e) Optimized structure of Yb@$C_s(6)$-C_{82} (left, side view; right, top view).

the two isomers fairly stable for C_{80}^{6-}.[49−52] Other cage structures of C_{80} are rare: Ti_2@C_{80}[53] was recently disclosed as a cluster EMF, Ti_2C_2@C_{78};[54] the hetero di-EMF ScPr@C_{80}, which was reported to bear a C_{2v} cage structure by unconvincing ^{13}C NMR results,[30] is also putatively a metal carbide EMF ($ScPrC_2$@C_{78}). Only one example of mono-EMFs with a C_{80} cage has been reported to date, i.e., La@C_{80}, captured as La@$C_{80}(C_4H_3Cl_2)$, whose cage structure was established unambiguously using single crystallographic determination to be the $C_{2v}(3)$ isomer.[33] However, because pristine La@C_{80} is not obtainable as a consequence of its insolubility and high reactivity, Yb@C_{80} shown here is the first example of pristine mono-EMFs based on a C_{80} cage whose cage structure is clearly elucidated.

Figure 1a presents the ^{13}C NMR spectrum of Yb@C_{80}, where 23 signals are observed, 17 with full intensity and six with half. This pattern is unambiguously assigned to the $C_{2v}(3)$ cage.[40] Additionally, the calculated ^{13}C NMR spectrum of Yb@$C_{2v}(3)$-C_{80} (Figure 1b) agrees well with the observed one. The optimized structure of Yb@C_{80} is shown in Figure 1c as viewed from two orthogonal directions. It is apparent that the Yb atom is not in the center of the cage but is located close to a [6,6]-bond along the C_2 axis, indicative of strong metal−cage interactions.

It is still surprising that only one isomer of Yb@C_{80} has been isolated. Actually, one stable isomer of other divalent M@C_{80} (M = Ca, Sr, Ba, Sm, Eu) has been reported, but no structural determination has been presented.[14,15,55] Here, the similarity of their electronic absorption spectra to that of Yb@C_{80} indicates that all these species have the same $C_{2v}(3)$ cage structure.

It is interesting that Yb@C_{80} adopts the same cage structure as La@C_{80} and that this cage differs from the structures of other C_{80}-based fullerene allotropes. Because Yb donates two electrons to the carbon cage whereas La gives three, the same $C_{2v}(3)$ cage seems not merely a result of electronic configuration but also a probable consequence of the geometrical effect of the metal atom. In view of the fact that computational results showed that the $D_{5h}(6)$ and $C_{2v}(5)$ isomers are always more stable than $C_{2v}(3)$ for either C_{80}^{2-} or C_{80}^{3-} but these cages have never been obtained,[33] it can be inferred that a pure electronic consideration is not sufficient to describe the EMF formation process. Herein we propose a metal-templated growth process (MTGP) of EMFs: aside from the electronic configuration of EMFs, which is a thermodynamic factor for determining the stability and cage structures of EMFs, the existence and location of metals within the cage are also critical to control the formation of EMF kinetically (*vide infra*).

3.1.3. Cage Structures of Yb@C_{82}(I, II, III). C_{82} has nine IPR-satisfying cages. However, because of its low production yield in soot, only the $C_2(3)$ isomer has been isolated and characterized.[56,57] It was astonishing, at least initially, that the $C_{2v}(9)$ cage, together with the $C_s(6)$ isomer, becomes the most abundant and stable when encapsulating a trivalent lanthanide metal (Sc, Y, La, Ce, etc.).[21−26]

Three isomers of Yb@C_{82} were isolated and characterized structurally. The ^{13}C NMR spectrum of Yb@C_{82}(I) shown in Figure 2a contains 44 signals (38 with full intensity and six with half), which corresponds to any of the three C_s-symmetric

(49) Kobayashi, K.; Nagase, S.; Akasaka, T. *Chem. Phys. Lett.* **1995**, *245*, 230–236.
(50) Popov, A. A.; Dunsch, L. *J. Am. Chem. Soc.* **2007**, *129*, 11835–11849.
(51) Chaur, M. N.; Valencia, R.; Rodriguez-Fortea, A.; Poblet, J. M.; Echegoyen, L. *Angew. Chem., Int. Ed.* **2009**, *48*, 1425–1428.
(52) Campanera, J. M.; Bo, C.; Poblet, J. M. *Angew. Chem., Int. Ed.* **2005**, *44*, 7230–7233.
(53) Cao, B. P.; Hasegawa, M.; Okada, K.; Tomiyama, T.; Okazaki, T.; Suenaga, K.; Shinohara, H. *J. Am. Chem. Soc.* **2001**, *123*, 9679–9680.
(54) Tan, K.; Lu, X. *Chem. Commun.* **2005**, 4444–4446.
(55) Sun, B. Y.; Inoue, T.; Shimada, T.; Okazaki, T.; Sugai, T.; Suenaga, K.; Shinohara, H. *J. Phys. Chem. B* **2004**, *108*, 9011–9015.
(56) Kikuchi, K.; Nakahara, N.; Wakabayashi, T.; Suzuki, S.; Shiromaru, H.; Miyake, Y.; Saito, K.; Ikemoto, I.; Kainosho, M.; Achiba, Y. *Nature* **1992**, *357*, 142–145.
(57) Sun, G. Y.; Kertesz, M. *J. Phys. Chem. A* **2001**, *105*, 5468–5472.

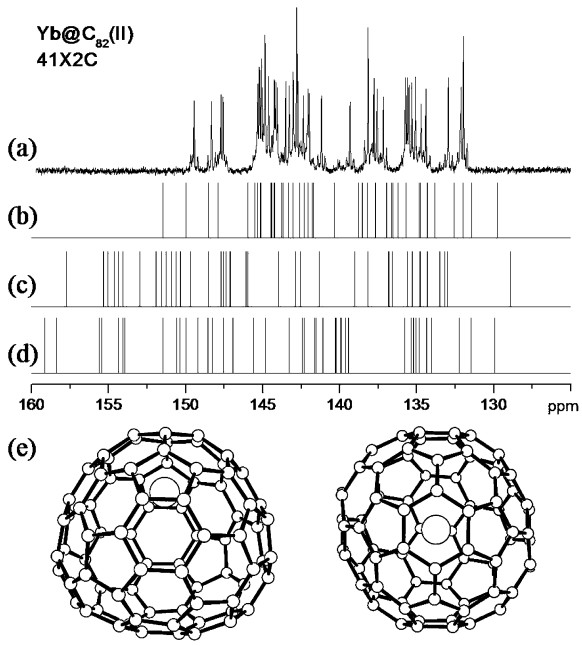

Figure 3. (a) ^{13}C NMR spectrum of Yb@C_{82}(II) with 41 equal-intensity peaks (41 × 2C pattern). The obviously higher peaks are doublets due to coincidental overlap. (b) Calculated ^{13}C NMR spectrum of Yb@C_2(5)-C_{82}, which is the most stable C_2 isomer. (c) Calculated ^{13}C NMR spectrum of Yb@C_2(1)-C_{82}, which is 72.6 kJ/mol less stable than the C_2(5) isomer. (d) Calculated ^{13}C NMR spectrum of Yb@C_2(3)-C_{82}, which is 79.8 kJ/mol less stable than the C_2(5) isomer. (e) Optimized structure of Yb@C_2(5)-C_{82} (left, side view; right, top view).

cages,[40] so that theoretical calculations are performed to determine the cage structure of Yb@C_{82}(I) finally. The calculated results showed that when encapsulating a divalent Yb atom that transfers two electrons to the cage, the C_s(6) isomer becomes 52.5 and 96.3 kJ/mol more stable than the C_s(4) and C_s(2) isomers, respectively (Figure S14). Furthermore, the calculated ^{13}C NMR spectrum of Yb@C_s(6)-C_{82} (Figure 2b) resembles the experimental result, but the calculated spectra of the other two (Figure 2c,d) exhibit several deshielded resonances at higher than 150 ppm. Accordingly, it is sound to assign the C_s(6) cage to Yb@C_{82}(I). The optimized structure of Yb@C_{82}(I) portrayed in Figure 2e discloses that the Yb atom sits under a [6,6]-bond on the mirror plane, as found for Eu@C_{82}(I) by the XRD/MEM/Rietveld method.[58] It is noteworthy that this cage structure is also found for the minor isomer of trivalent M@C_{82} (M = La, Ce, Pr, Gd, etc.).[22−26]

The spectrum with 41 equal-intensity peaks (Figure 3a) confirms a C_2 symmetry of Yb@C_{82}(II). Similarly, three IPR isomers of C_{82} have a C_2 symmetry;[40] theoretical calculations revealed that for Yb@C_2-C_{82} the C_2(5) isomer is more stable than the C_2(1) and C_2(3) isomers by 72.6 and 79.8 kJ/mol, respectively (Figure S15). Moreover, the calculated ^{13}C NMR spectrum of Yb@C_2(5)-C_{82} agrees well with the observed one, but many downfield signals between 152 and 160 ppm are calculated for the other two (Figure 3b,c,d). Consequently, the cage structure of Yb@C_{82}(II) is reasonably assigned to C_2(5). As presented in Figure 3e in the optimized structure of Yb@C_2(5)-C_{82}, the Yb atom tends to reside under a hexagonal

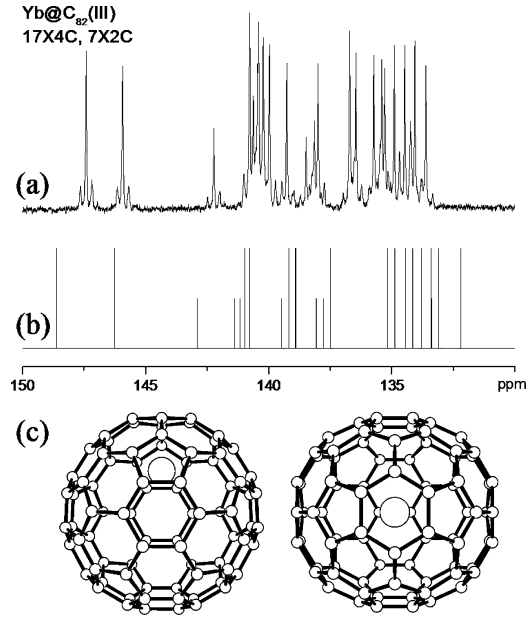

Figure 4. (a) ^{13}C NMR spectrum of Yb@C_{82}(III) showing a 17 × 4C, 7 × 2C pattern. (b) Calculated ^{13}C NMR spectrum of Yb@C_{2v}(9)-C_{82}. (c) Optimized structure of Yb@C_{2v}(9)-C_{82} (left, side view; right, top view).

ring along the C_2 axis. This cage is only found for divalent M@C_{82} and differs from the only isolated isomer of empty C_2(3)-C_{82}.

The spectrum of Yb@C_{82}(III) consists of 24 peaks in the aromatic region, among which 17 have full intensity and seven have half-intensity (Figure 4a). This pattern evidently corresponds to the C_{2v}(9) cage, which is also the cage of the major isomer of trivalent M@C_{82} (M = Sc, Y, La, Ce, Pr, Gd, etc.).[21−26,59] Furthermore, the calculated spectrum shown in Figure 4b agrees perfectly with the observed one, which further corroborates the assignment. The optimized molecule structure of Yb@C_{82}(III) is presented in Figure 4c. The Yb atom is located under a hexagonal ring along the C_2 axis, a case similar to the position of the trivalent metal atom in M@C_{82} (M = Sc, Y, La, Ce, Pr, Gd).[21,29,60−62] Previous XRD/MEM/Rietveld results of M@C_{2v}(9)-C_{82} (M = Eu and Gd) have proposed that the metal atom is located over a [6,6]-bond opposite the hexagonal ring along the C_2 axis.[58] However, both theoretical calculations and X-ray results of Gd@C_{82} (or its derivative) confirmed that the Gd atom is sitting under a hexagonal ring.[61] Consequently, it is reasonable to conclude that the Eu atom is also sitting under a hexagonal ring along the C_2 axis, which is expected to be finally proved by single crystallographic results in the near future.

Actually three or four isomers of other divalent M@C_{82} (M = Ca, Sr, Ba, Sm, Eu, Tm) have been isolated,[13−16] and the isomers of M@C_{82} (M = Ca, Tm) were determined by Kodama

(58) (a) Sun, B. Y.; Sugai, T.; Nishibori, E.; Iwata, K.; Sakata, M.; Takata, M.; Shinohara, H. *Angew. Chem., Int. Ed.* **2005**, *44*, 4568–4571. (b) Nishibori, E.; Iwata, K.; Sakata, M.; Takata, M.; Tanaka, H.; Kato, H.; Shinohara, H. *Phys. Rev. B* **2004**, *69*, 113412.

(59) Lu, X.; Shi, Z. J.; Sun, B. Y.; He, X. R.; Gu, Z. N. *Fullerenes, Nanotubes, Carbon Nanostruct.* **2005**, *13*, 13–20.

(60) Maeda, Y.; et al. *J. Am. Chem. Soc.* **2004**, *126*, 6858–6859.

(61) (a) Mizorogi, N.; Nagase, S. *Chem. Phys. Lett.* **2006**, *431*, 110–112. (b) Liu, L.; Gao, B.; Chu, W. S.; Chen, D. L.; Hu, T. D.; Wang, C. R.; Dunsch, L.; Marcelli, A.; Luo, Y.; Wu, Z. Y. *Chem. Commun.* **2008**, 474–476. (c) Akasaka, T.; et al. *J. Am. Chem. Soc.* **2008**, *130*, 12840–12841.

(62) Lu, X.; Nikawa, H.; Feng, L.; Tsuchiya, T.; Maeda, Y.; Akasaka, T.; Mizorogi, N.; Slanina, Z.; Nagase, S. *J. Am. Chem. Soc.* **2009**, *131*, 12066–12067.

et al.[27,63] to bear similar cage symmetries to those found in Yb@C_{82}(I, II, III) with ^{13}C NMR spectrometry. However, no exact assignments of the C_2 and C_s isomers were made for M@C_{82} (M = Ca, Tm) in these reports. Here we have accurately assigned the cage structures of Yb@C_{82}(I, II, III) so that the cage structures of other divalent M@C_{82} (M = Ca, Sr, Ba, Sm, Eu, Tm)[13−16] can be deduced from the similarities of their absorption spectra to that of corresponding Yb@C_{82} isomers.

It is informative to compare the cage structures of C_{82}-based EMFs encapsulating different numbers of metal atoms. As described, the C_{2v}(9)-C_{82} and C_s(6)-C_{82} cages are adopted by trivalent M@C_{82},[21−26] and the two cages remain suitable for hosting a divalent metal, e.g., Tm or Yb, plus a C_2(5)-C_{82} cage.[27,63] In contrast, two metal atoms or a bimetallic carbide cluster prefers to template the C_{3v}(8) cage; for example, Y_2@C_{82} and Y_2C_2@C_{82} and the C_{2v}(9)-C_{82} cage are less abundantly formed.[11] Surprisingly, a TNT cluster tends to template a non-IPR cage of C_s(39663), forming, for example, Gd_3N@C_{82}.[64] These experimental results implied again that the formation of EMFs not only is determined by the electronic configuration of the resulting EMFs but also depends on the number of internal metals. One metal atom generally engenders the formation of three or four cage isomers with lower cage symmetries, whereas two metal atoms would template the isomers with higher symmetries (C_{3v} and C_{2v}). Regarding the larger cluster Gd_3N, strong interactions between the encaged metals and the cage carbon specify only one cage isomer, which might be a combined influence of geometrical templating and electronic dictation. In recent years, the nexus of efforts to elucidate EMFs has moved from conventional EMFs to TNT EMFs.[6−8,50−52] Our results show a systematic investigation of mono-EMFs, which are helpful to understand the structures, properties, and formation mechanisms of EMFs.

3.1.4. Cage Structures of Yb@C_{84}(II, III, IV). Because of the high production yield in soot (the third most abundant fullerene) and isomeric diversity (24 IPR-satisfying isomers), isolated isomers of empty C_{84} are quite numerous.[65] The cage connectivities of the D_{2d}(23),[66] C_2(11),[67] C_s(14),[68] D_2(22),[69] and C_s(16)[69] isomers have been disclosed unambiguously using X-ray single crystallography. Moreover, a ^{13}C NMR study has revealed two additional C_{84} isomers with an unidentified D_2 cage and the D_{2d}(4) cage and a mixture containing the two isomers of D_{3d}(19) and D_{6h}(24).[70]

In all, four isomers were isolated for Yb@C_{84}. However, the extremely low production yield of Yb@C_{84}(I) has hindered the pursuit of its high-quality ^{13}C NMR spectrum with a good S/N ratio. Nevertheless, a total of less than 20 detectable peaks in the range 120−160 ppm indicates a relatively high cage symmetry (Figure S10).[40]

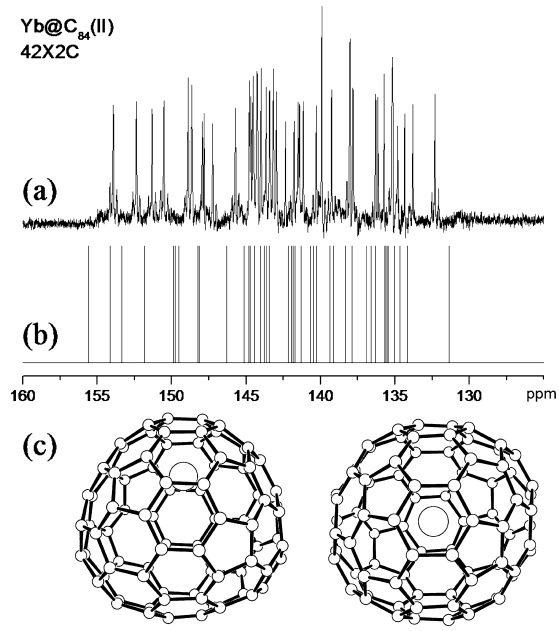

Figure 5. (a) ^{13}C NMR spectrum of Yb@C_{84}(II) displaying 42 equal-intensity peaks (42 × 2C pattern). (b) Calculated ^{13}C NMR spectrum of Yb@C_2(13)-C_{84}, which is the most stable C_2 isomer. (c) Optimized structure of Yb@C_2(13)-C_{84} (left, side view; right, top view).

The ^{13}C NMR spectrum of Yb@C_{84}(II) is presented in Figure 5a. The 42 measured resonances with equal intensity are in accord with all five C_2-symmetric cages,[40] so that theoretical calculations were conducted to make a final decision. The results showed that the C_2(13) isomer is at least 36.6 kJ/mol more stable than the other four C_2 isomers (Figure S16). Furthermore, the calculated spectrum of Yb@C_2(13)-C_{84} (Figure 4b) is in good agreement with the observed one. Consequently, the cage structure of Yb@C_{84}(II) is assigned to C_2(13). Its optimized structure in Figure 5c shows that the Yb atom is located under a hexagonal ring along the C_2 axis. It is noteworthy that this is a new fullerene allotrope that has never been reported for either empty fullerenes or EMFs.

As presented in Figure 6a, Yb@C_{84}(III) displays 84 ^{13}C NMR peaks in all. Consequently, its cage structure can be assigned unambiguously to the C_1(12) isomer because this is the only one having C_1 symmetry among the 24 IPR C_{84} isomers.[40] Further corroboration of the assignment is the consistency between the calculated ^{13}C NMR spectrum (Figure 6b) and the experimental one. This cage structure is surprising because no fullerene isomer with a C_1 symmetry has been reported before. Figure 6c shows the optimized structure of Yb@C_1(12)-C_{84} as viewed from two different directions. The Yb atom is located close to a [6,6]-bond junction instead of sitting under a hexagonal ring.

Yb@C_{84}(IV) also displays 42 ^{13}C NMR resonances with equal intensity (Figure 7a), indicative of a C_2 symmetry.[40] Because the most stable C_2(13)-C_{84} cage has already been assigned to Yb@C_{84}(II), the second most stable isomer, C_2(9)-C_{84}, which is 36.6 kJ/mol higher in energy, is selected as the most probable candidate for Yb@C_{84}(IV). However, the calculated ^{13}C NMR spectrum of Yb@C_2(9)-C_{84} displays a highly deshielded resonance at 165 ppm and an abnormal upfield signal at 123 ppm (Figure 7b), which evidently conflicts with the experimental results. The third most stable

(63) Kodama, T.; Fujii, R.; Miyake, Y.; Sakaguchi, K.; Nishikawa, H.; Ikemoto, I.; Kikuchi, K.; Achiba, Y. *Chem. Phys. Lett.* **2003**, *377*, 197–200.
(64) Mercado, B. Q.; Beavers, C. M.; Olmstead, M. M.; Chaur, M. N.; Walker, K.; Holloway, B. C.; Echegoyen, L.; Balch, A. L. *J. Am. Chem. Soc.* **2008**, *130*, 7854–7855.
(65) Thilgen, C.; Diederich, F. *Chem. Rev.* **2006**, *106*, 5049–5135.
(66) Balch, A. L.; Ginwalla, A. S.; Lee, J. W.; Noll, B. C.; Olmstead, M. M. *J. Am. Chem. Soc.* **1994**, *116*, 2227–2228.
(67) Kareev, I. E.; Kuvychko, I. V.; Shustova, N. B.; Lebedkin, S. F.; Bubnov, V. P.; Anderson, O. P.; Popov, A. A.; Boltalina, O. V.; Strauss, S. H. *Angew. Chem., Int. Ed.* **2008**, *47*, 6204–6207.
(68) Epple, L.; Amsharov, K.; Simeonov, K.; Dix, I.; Jansen, M. *Chem. Commun.* **2008**, 5610–5612.
(69) Tamm, N. B.; Sidorov, L. N.; Kemnitz, E.; Troyanov, S. I. *Chem.—Eur. J.* **2009**, *15*, 10486–10492.
(70) Tagmatarchis, N.; Avent, A. G.; Prassides, K.; Dennis, T. J. S.; Shinohara, H. *Chem. Commun.* **1999**, 1023–1024.

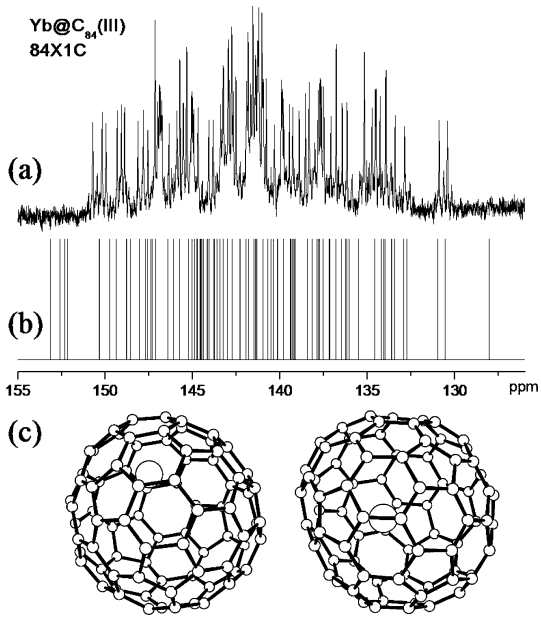

Figure 6. (a) ^{13}C NMR spectrum of Yb@C_{84}(III) showing 84 equal-intensity peaks (84 × 1C pattern). (b) Calculated ^{13}C NMR spectrum of Yb@C_1(12)-C_{84}. (c) Optimized structure of Yb@C_1(12)-C_{84} (left, side view; right, top view).

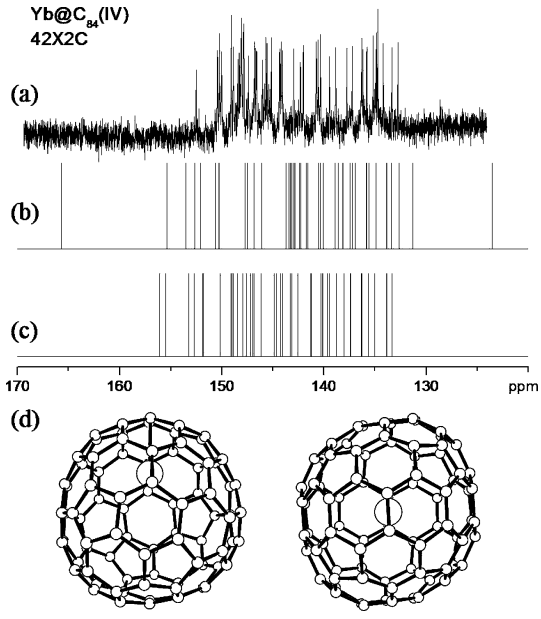

Figure 7. (a) ^{13}C NMR spectrum of Yb@C_{84}(IV) with 42 equal-intensity peaks (42 × 2C pattern). (b) Calculated ^{13}C NMR spectrum of Yb@C_2(9)-C_{84}, which is 36.6 kJ/mol less stable than the C_2(13) isomer. (c) Calculated ^{13}C NMR spectrum of Yb@C_2(11)-C_{84}, which is 54.2 kJ/mol less stable than the C_2(13) isomer. (d) Optimized structure of Yb@C_2(11)-C_{84} (left, side view; right, top view).

isomer, Yb@C_2(11)-C_{84}, however, exhibits a ^{13}C NMR spectrum that very closely resembles the observed one and is only 17.6 kJ/mol higher in energy than Yb@C_2(9)-C_{84}. The remaining two C_2 isomers, C_2(2)-C_{84} and C_2(8)-C_{84}, are unlikely to be possible because they are highly unstable for Yb@C_{84} (Figure S16). Consequently, the C_2(11) cage is reasonably assigned to Yb@C_{84}(IV), and the results are consistent with the relative abundances of Yb@C_{84}(II) and Yb@C_{84}(IV) (8:3, Table 1). The structure of Yb@C_2(11)-C_{84} in Figure 7d shows that the Yb atom tends to situate under a [6,6]-bond junction because no hexagonal ring exists along this C_2 axis.

Again, we make a structural comparison of these Yb@C_{84} isomers with other C_{84}-based EMFs with respect to the number of encapsulated metals. For mono-EMFs M@C_{84}, two isomers of Ca@C_{84} were isolated in 1996[13] and three isomers of Sm@C_{84} were obtained in 2000,[15] but no structural characterizations were reported for them. Because all are divalent EMFs, now it can be concluded that Ca@C_{84}(I, II) have the same cages as Yb@C_{84}(II, III), respectively, and Sm@C_{84}(I, II, III) have the respective cage structures of Yb@C_{84}(II, III, IV), by simply comparing their respective UV−vis−NIR spectra with those of Yb@C_{84} isomers. Examples of M_2@C_{84} are truly scarce. The previously assigned Sc_2@C_{84}[71] was recently found to be a cluster EMF, Sc_2C_2@C_{82}.[72] Although several isomers of M_2@C_{84} (M = Ti, Er) have been isolated, no structural evidence is available for any of them.[73] For cluster EMFs with a C_{84} cage, the Sc_2C_2 unit prefers the D_{2d}(23) cage,[20] which is also the most abundant one for empty C_{84}, while an M_3N cluster (M = Tb,[74] Gd,[75] Tm[75]) tends to template the non-IPR C_s(51356)-C_{84} cage. These results again lead us to conclude that the formation of EMFs kinetically involves a templating effect of the metal during the arc discharge process because different numbers of metals normally result in different cage structures. As a consequence of this speculation, we can expect that trivalent M@C_{84} isomers having the same cage structures as Yb@C_{84}(II, III, IV) will be found in future studies, preferably in the form of their derivatives.[31−33]

The similarity of the cage structures of Yb@C_2(5)-C_{82} and Yb@C_2(13)-C_{84} provides strong support for the metal-templated growth process of EMFs. As shown in Figure 8, insertion of two equivalent C atoms (emphasized in blue) into the framework of Yb@C_2(5)-C_{82} forms Yb@C_2(13)-C_{84}. More convincingly, the two "extra" carbon atoms of Yb@C_2(13)-C_{84} are added to the place most distant from the Yb atom. These indicate clearly that the growth of Yb@C_2(13)-C_{84} from the framework of Yb@C_2(5)-C_{82} is templated by the Yb atom. Moreover, it must be remarked that in both structures the Yb atoms are located under a hexagonal ring along the C_2 axis, which is expected to be the most preferred position for the metal atom in mono-EMFs. Actually, a similar structural transformation from non-IPR Gd_3N@C_s(39663)-C_{82}[64] to Gd_3N@C_s(51365)-C_{84}[75] has been reported, which could constitute additional evidence of the MTGP.

3.2. Electrochemical Properties. High sensitivity and low cost have made electrochemical methods one of the most effective and popular means for elucidating the structures and properties

(71) Takata, M.; Nishibori, E.; Umeda, B.; Sakata, M.; Yamamoto, E.; Shinohara, H. *Phys. Rev. Lett.* **1997**, *78*, 3330–3333.
(72) (a) Iiduka, Y.; Wakahara, T.; Nakajima, K.; Tsuchiya, T.; Nakahodo, T.; Maeda, Y.; Akasaka, T.; Mizorogi, N.; Nagase, S. *Chem. Commun.* **2006**, 2057–2059. (b) Iiduka, Y.; Wakahara, T.; Nakajima, K.; Nakahodo, T.; Tsuchiya, T.; Maeda, Y.; Akasaka, T.; Yoza, K.; Liu, M. T. H.; Mizorogi, N.; Nagase, S. *Angew. Chem., Int. Ed.* **2007**, *46*, 5562–5564.
(73) (a) Cao, B. P.; Suenaga, K.; Okazaki, T.; Shinohara, H. *J. Phys. Chem. B* **2002**, *106*, 9295–9298. (b) Tagmatarchis, N.; Aslanis, E.; Shinohara, H.; Prassides, K. *J. Phys. Chem. B* **2000**, *104*, 11010–11012.
(74) Beavers, C. M.; Zuo, T. M.; Duchamp, J. C.; Harich, K.; Dorn, H. C.; Olmstead, M. M.; Balch, A. L. *J. Am. Chem. Soc.* **2006**, *128*, 11352–11353.
(75) Zuo, T.; Walker, K.; Olmstead, M. M.; Melin, F.; Holloway, B. C.; Echegoyen, L.; Dorn, H. C.; Chaur, M. N.; Chancellor, C. J.; Beavers, C. M.; Balch, A. L.; Athans, A. J. *Chem. Commun.* **2008**, 1067–1069.

Table 1. Redox Potentials (V vs Fc/Fc^+),[a] Electrochemical Bandgaps (V), HOMO/LUMO Values (eV), Ionization Potentials, and Electron Affinities (eV) of Different EMFs, and Relative Yields of $Yb@C_{2n}$ (n = 40, 41, 42)

species	$^{ox}E_2$	$^{ox}E_1$	$^{red}E_1$	$^{red}E_2$	$^{red}E_3$	$^{red}E_4$	ΔE ($^{ox}E_1$-$^{red}E_1$)	HOMO/LUMO	Ip/Ea	relative yield
$Yb@C_{80}$	0.78[b]	0.34	−0.89	−1.27	−1.87	−2.13	1.23	−4.98/−3.60	6.39/2.96	0.6
$Yb@C_{82}$(I)		0.34	−0.62	−0.92	−1.81	−2.01	0.96	−5.29/−3.92	6.68/3.27	0.5
$Yb@C_{82}$(II)	0.90[b]	0.38	−0.86	−0.98	−1.50	−1.87	1.24	−5.19/−3.55	6.58/2.91	0.8
$Yb@C_{82}$(III)		0.61	−0.46	−0.78	−1.60	−1.90	1.07	−5.48/−4.04	6.87/3.39	1
$Yb@C_{84}$(I)	0.53	0.12	−0.76	−1.06	−1.63[c]		0.88			0.01
$Yb@C_{84}$(II)		0.46	−0.95	−1.16	−1.50	−1.86	1.41	−5.27/−3.46	6.65/2.84	0.8
$Yb@C_{84}$(III)	0.68	0.22	−0.76	−0.94	−1.76	−1.97	0.98	−5.00/−3.63	6.38/3.00	0.5
$Yb@C_{84}$(IV)	0.48	0.19	−0.85	−1.14	−1.70	−2.06	1.04	−4.88/−3.50	6.27/2.87	0.3
$La@C_{2v}(9)$-C_{82}[d]	1.07	0.07	−0.42	−1.37	−1.53	−2.26	0.49	−4.81/−3.39	6.19/3.38	
$La@C_s(6)$-C_{82}[e]	1.08	−0.07	−0.47	−1.40	−2.01	−2.40	0.40	−4.67/−3.27	6.05/3.21	
$La_2@I_h(7)$-C_{80}[f]	0.95	0.56	−0.31	−1.71	−2.13[b]		0.87	−5.40/−4.01		
$Sc_3N@I_h(7)$-C_{80}[f]	1.09	0.62	−1.22	−1.59	−1.90		1.88	−5.48/−3.14		

[a] Half-cell potentials in ODCB unless otherwise noted. [b] DPV value. [c] Two-electron process. [d] Ref 23. [e] Ref 83. [f] Ref 84.

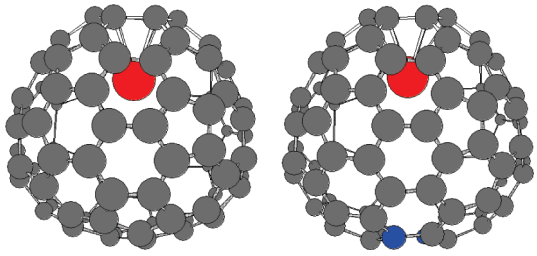

Figure 8. Comparison of the structures of $Yb@C_2(5)$-C_{82} (left) and $Yb@C_2(13)$-C_{84} (right). Gray, C; red, Yb. The two "extra" C atoms of $Yb@C_2(13)$-C_{84} are highlighted in blue; the bonds between Yb and the cage carbons of the adjacent hexagonal ring are shown in both structures to ease comprehension.

of EMFs and their derivatives.[7,76] Results showed that trivalent mono-EMFs, such as $M@C_{82}$ (M = Y, La, Ce, Pr, Gd, etc.), have a very negative first oxidation potential ($^{ox}E_1$) and a highly positive first reduction potential ($^{red}E_1$). Therefore, they have an extremely small electrochemical bandgap ($\Delta E = {}^{ox}E_1 - {}^{red}E_1$), normally less than 0.5 V.[7,22−26,77] In contrast, the $^{ox}E_1$ values of di-EMFs, e.g., $M_2@C_{2n}$ (M = La, Ce; n = 36, 39, 40), are rather positive and their bandgaps are accordingly larger, but still smaller than 1.0 V.[78] However, the members of the TNT family normally possess both higher oxidation and reduction potentials, with wider bandgaps ranging from 1.38 V for $Ce_3N@C_{88}$[79] to 2.08 V for $Tm_3N@C_{80}$.[48] In summary, all these EMFs contain trivalent metal atom(s). Consequently, it is particularly desirable to investigate the electrochemical properties of divalent EMFs because the transferred charges play an important role in determining the structures and properties of EMFs.

Unfortunately, previous electrochemical investigations of divalent $M@C_{2n}$ (M = Ca,[80] Sm,[81] and Yb[18]) presented only their reduction processes but failed in observing the oxidation steps, which has led to the assumption that they are large energy gap materials.[7] The previous electrochemical studies were performed in a mixed solution of acetonitrile/toluene (v/v = 1:4),[18,80,81] which was suitable for obtaining even the sixth reduction step of C_{60}.[82] However, this mixture is not commonly adopted for the electrochemical studies of EMFs because of its poor capacity of solubilizing EMFs. Instead, 1,2-dichlorobenzene is more frequently used, and numerous redox potential values of EMFs have been obtained using this solvent.[7,76−79]

In this study, the unexplored oxidation processes of divalent EMFs were achieved in ODCB. The results demonstrated that all isomers of $Yb@C_{2n}$ (n = 40, 41, 42) display one or two oxidation steps together with four reversible reduction steps within the solvent window. Their redox behaviors are characteristic of divalent EMFs and strongly corroborate the electronic structure of $Yb^{2+}@C_{2n}{}^{2-}$.

The cyclic voltammograms of $Yb@C_{80}$ and $Yb@C_{82}$ (I, II, III) are portrayed in Figure 9, and the corresponding differential pulse voltammograms are shown in Figure S5. As marked with solid dots, $Yb@C_{80}$ displays one quasi-reversible oxidation step and four reversible reduction steps, even at a very low scan rate (20 mV/s). Similarly, the three isomers of $Yb@C_{82}$ all show one (quasi-)reversible oxidation step and four reversible reduction steps under identical conditions. A likely irreversible second oxidation step is also visible, but it is not well identified and will not be discussed further. Similar to the results observed in acetonitrile/toluene by Xu et al.,[18] the first two reduction steps of each compound are mutually close, as are the following two, but the gap separating the second and the third is larger. These results strongly corroborate their closed-shell electronic configuration with nondegenerate low-lying LUMO and accessible

(76) (a) Feng, L.; Wakahara, T.; Nakahodo, T.; Tsuchiya, T.; Piao, Q.; Maeda, Y.; Lian, Y.; Akasaka, T.; Horn, E.; Yoza, K.; Kato, T.; Mizorogi, N.; Nagase, S. *Chem.—Eur. J.* **2006**, *12*, 5578–5586. (b) Herranz, M. A.; Diederich, F.; Echegoyen, L. *Eur. J. Org. Chem.* **2004**, *229*, 9–2316. (c) Lukoyanova, O.; Cardona, C. M.; Altable, M.; Filippone, S.; Domenech, A. M.; Martin, N.; Echegoyen, L. *Angew. Chem., Int. Ed.* **2006**, *45*, 7430–7433. (d) Cardona, C. M.; Elliott, B.; Echegoyen, L. *J. Am. Chem. Soc.* **2006**, *128*, 6480–6485. (e) Chaur, M. N.; Athans, A. J.; Echegoyen, L. *Tetrahedron* **2008**, *64*, 11387–11393. (f) Elliott, B.; Yu, L.; Echegoyen, L. *J. Am. Chem. Soc.* **2005**, *127*, 10885–10888.

(77) Suzuki, T.; Maruyama, Y.; Akasaka, T.; Ando, W.; Kobayashi, K.; Nagase, S. *J. Am. Chem. Soc.* **1994**, *116*, 1359–1363.

(78) (a) Yamada, M.; Feng, L.; Wakahara, T.; Tsuchiya, T.; Maeda, Y.; Lian, Y. F.; Kako, M.; Akasaka, T.; Kato, T.; Kobayashi, K.; Nagase, S. *J. Phys. Chem. B* **2005**, *109*, 6049–6051. (b) Yamada, M.; Wakahara, T.; Nakahodo, T.; Tsuchiya, T.; Maeda, Y.; Akasaka, T.; Yoza, K.; Horn, E.; Mizorogi, N.; Nagase, S. *J. Am. Chem. Soc.* **2006**, *128*, 1402–1403. (c) Yamada, M.; Mizorogi, N.; Tsuchiya, T.; Akasaka, T.; Nagase, S. *Chem.—Eur. J.* **2009**, *15*, 9486–9493. (d) Yamada, M.; Wakahara, T.; Tsuchiya, T.; Maeda, Y.; Akasaka, T.; Mizorogi, N.; Nagase, S. *J. Phys. Chem. A* **2008**, *112*, 7627–7631. (e) Cao, B.; Nikawa, H.; Nakahodo, T.; Tsuchiya, T.; Maeda, Y.; Akasaka, T.; Sawa, H.; Slanina, Z.; Mizorogi, N.; Nagase, S. *J. Am. Chem. Soc.* **2008**, *130*, 983–989.

(79) Chaur, M. N.; Melin, F.; Ashby, J.; Elliott, B.; Kumbhar, A.; Rao, A. M.; Echegoyen, L. *Chem.—Eur. J.* **2008**, *14*, 8213–8219.

(80) Zhang, Y.; Xu, J. X.; Hao, C.; Shi, Z. J.; Gu, Z. N. *Carbon* **2006**, *44*, 475–479.

(81) Liu, J.; Shi, Z. J.; Gu, Z. N. *Chem. Asian J.* **2009**, *4*, 1703–1711.

(82) Xie, Q. S.; Perezcordero, E.; Echegoyen, L. *J. Am. Chem. Soc.* **1992**, *114*, 3978–3980.

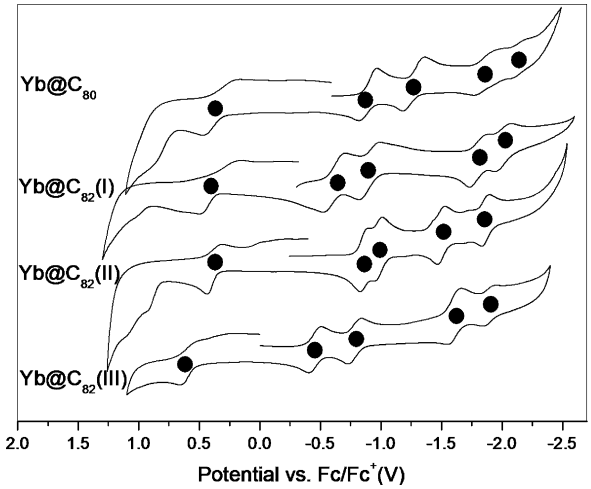

Figure 9. CV curves of Yb@C_{80}, Yb@C_{82}(I), Yb@C_{82}(II), and Yb@C_{82}(III) (from top to bottom). Each redox step is marked with a solid dot to aid comparison.

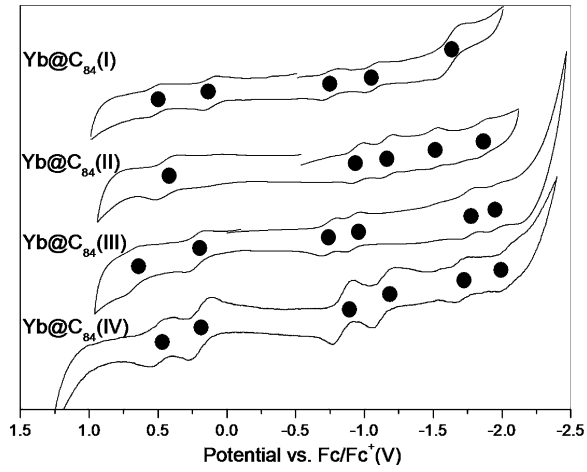

Figure 10. CV curves of Yb@C_{84}(I), Yb@C_{84}(II), Yb@C_{84}(III), and Yb@C_{84}(IV) (from top to bottom). Each redox step is marked with a solid dot to aid comparison. The third reduction of Yb@C_{84}(I) is a two-electron process, but is marked with only one solid dot.

LUMO+1 orbitals. These are consistent with the calculated HOMO/LOMO values presented in Table 1.

In sharp contrast with the fact that the electrochemical potentials of the two structural isomers of trivalent La@C_{82} are nearly identical (Table 1), the influence of the cage structures on the electrochemical potentials of Yb@C_{82}(I, II, III) is evident: the redox potentials of Yb@C_{82}(III) are shifted cathodically by 0.16−0.27 V compared with the corresponding values of Yb@C_{82}(I, II), which makes Yb@C_{82}(III) the best electron acceptor, but the worst donor. These results demonstrate clearly that the open-shell configuration of trivalent mono-EMFs has a prevailing influence on their electronic structures, whereas the influence of the cage structure is negligible.

The CV curves of Yb@C_{84}(I, II, III, IV) are depicted in Figure 10. When the cage becomes larger, the number of oxidation processes normally increases and the reversibility is also improved. Except Yb@C_{84}(II), which still has one oxidation step within the solvent window, Yb@C_{84}(I, III, IV) all display two reversible oxidation steps accompanying four reversible reduction processes. Particularly, the third and fourth reduction steps of Yb@C_{84}(I) are combined into a two-electron process, indicating a degenerate LUMO+1 orbital. Again, the first and second reduction potentials are mutually very close, as are the third and the fourth, but the gap between the third and the second is generally larger. Consequently, such electrochemical behaviors can be regarded as characteristic properties of divalent EMFs.

Isomeric influence on the electrochemical properties of Yb@C_{84}(I, II, III, IV) is also apparent. Briefly, Yb@C_{84}(II) is both the worst electron donor and the worst acceptor among the four isomers because it has the highest redox potentials (both $^{red}E_1$ and $^{ox}E_1$) and accordingly the largest bandgap.

The redox potentials, HOMO/LUMO, and Ip/Ea values of Yb@C_{2n} ($2n$ = 40, 41, 42) are presented in Table 1 together with data of some related EMFs for comparison. One important finding is that the redox potentials determined in ODCB are generally more negative than the corresponding values determined in acetonitrile/toluene, indicating a solvent effect on the electrochemical properties of EMFs. Similar behaviors of Sc_3N@C_{2n} (n = 39, 40) in different solvents were also observed in previous electrochemical studies.[85] Among the eight Yb-EMFs under study, Yb@C_{82}(III) is the best electron acceptor, and Yb@C_{84}(II) is the worst; Yb@C_{84}(I, III, IV) are the best electron donors, and Yb@C_{82}(III) is the worst electron donor, which is consistent with the calculated HOMO/LUMO and Ip/Ea values. The ΔE's of Yb@C_{2n} ($2n$ = 40, 41, 42), ranging from 0.88 V for Yb@C_{84}(I) to 1.41 V for Yb@C_{84}(II), are markedly larger than the values of trivalent M@C_{82} (M = Y, La, Ce, Pr, Gd) with open-shell configurations, but generally smaller than those of TNT EMFs. Furthermore, it can be concluded that a larger bandgap normally corresponds to a higher production yield of the Yb@C_{2n} isomers.

Finally, the electrochemical properties of Yb@C_{84}(II) are compared with those of Yb@C_{82}(II) because they have similar cage structures with the same Yb atoms (refer to Figure 8). Each has one reversible oxidation potential and four reduction potentials, but the $^{ox}E_1$ of the bigger cage is more positive than the value of the smaller one, and the $^{red}E_1$ and $^{red}E_2$ are more negative. These result in a larger bandgap for the larger cage. However, the $^{red}E_3$ and $^{red}E_4$ of the two species are respectively identical, indicating that only the levels of HOMO and LUMO are changed by the insertion of two "extra" carbons (Figure 8), whereas the LUMO+1 is unaffected.

4. Conclusion

In combination with theoretical calculations, ^{13}C NMR spectrometry has assigned the cage structures of a series of ^{13}C-enriched ytterbium EMFs: Yb@C_{2v}(3)-C_{80}, Yb@C_s(6)-C_{82}, Yb@C_2(5)-C_{82}, Yb@C_{2v}(9)-C_{82}, Yb@C_2(13)-C_{84}, Yb@C_1(12)-C_{84}, and Yb@C_2(11)-C_{84}. It is noteworthy that the cage structures of the C_{80} and C_{82} isomers have only been found for mono-EMFs; more importantly, the cage structures of C_2(13)-C_{84} and C_1(12)-C_{84} have never been reported for any fullerene allotrope. These results, together with the structural resemblance of Yb@C_2(13)-C_{84} to Yb@C_2(5)-C_{82}, indicate a metal-templat-

(83) Maeda, Y.; Miyashita, J.; Hasegawa, T.; Wakahara, T.; Tsuchiya, T.; Feng, L.; Lian, Y. F.; Akasaka, T.; Kobayashi, K.; Nagase, S.; Kako, M.; Yamamoto, K.; Kadish, K. M. *J. Am. Chem. Soc.* **2005**, *127*, 2143–2146.
(84) Iiduka, Y.; Ikenaga, O.; Sakuraba, A.; Wakahara, T.; Tsuchiya, T.; Maeda, Y.; Nakahodo, T.; Akasaka, T.; Kako, M.; Mizorogi, N.; Nagase, S. *J. Am. Chem. Soc.* **2005**, *127*, 9956–9957.
(85) (a) Zhang, L.; Chen, N.; Fan, L. Z.; Wang, C. R.; Yang, S. H. *J. Electroanal. Chem.* **2007**, *608*, 15–21. (b) Plonska-Brzezinska, M. E.; Athans, A. J.; Phillips, J. P.; Stevenson, S.; Echegoyen, L. *J. Electroanal. Chem.* **2008**, *614*, 171–174.

ing growth process of EMFs, which is expected to be one of the most important kinetic factors dictating the formation of EMFs. In addition, our electrochemical survey of $Yb@C_{2n}$ (n = 40, 41, 42) has revealed oxidation steps of divalent EMFs for the first time. All exhibit one or two (quasi)-reversible oxidation steps together with four reversible reduction processes, which show characteristic patterns of divalent EMFs. The cage structures have a marked effect on the electronic and electrochemical properties of these divalent EMFs. Further examinations show that their electrochemical bandgaps have a reasonable relation with the production yields. These results, which have elucidated the structures and properties of the poorly understood divalent EMFs and have provided valuable clues to the formation mechanism of EMFs, will be of fundamental importance for future work generating EMF-based functional materials.

Acknowledgment. We are grateful to Prof. Z. J. Shi at Peking University for providing $YbNi_2$ alloy. This work was supported in part by a Grant-in-Aid for Scientific Research on Innovative Areas (No. 20108001, "pi-Space"), a Grant-in-Aid for Scientific Research (A) (No. 20245006), the 21st Century COE Program, The Next Generation Super Computing Project (Nanoscience Project), Nanotechnology Support Project, and a Grant-in-Aid for Scientific Research on Priority Area (Nos. 20036008, 20038007) from the Ministry of Education, Culture, Sports, Science, and Technology of Japan.

Supporting Information Available: Complete refs 23, 41, 60, and 61c, HPLC profiles, mass spectra, vis−NIR spectra, DPV curves, expanded NMR spectra, summary of ^{13}C NMR chemical shifts, and relative stabilities of the $Yb@C_{2n}$ ($2n$ = 40, 41, 42) isomers. This material is available free of charge via the Internet at http://pubs.acs.org.

JA101131E